AGU PUBLICATIONS

Geophysical Research Letters

RESEARCH LETTER
10.1002/2013GL058373

Key Points:
- Predictions of forest change hampered by errors in current model formulations
- Remote Sensing can derive fine-scale information on the current ecosystem state
- Regional carbon fluxes can be constrained using remote sensing derived info

Supporting Information:
- Figure S1
- Figure S2
- Figure S3
- Figure S4
- Table S1
- Table S2
- Auxiliary material
- Supplement

Correspondence to:
P. R. Moorcroft,
paul_moorcroft@harvard.edu

Citation:
Antonarakis, A. S., J. W. Munger, and P. R. Moorcroft (2014), Imaging spectroscopy- and lidar-derived estimates of canopy composition and structure to improve predictions of forest carbon fluxes and ecosystem dynamics, *Geophys. Res. Lett.*, *41*, 2535–2542, doi:10.1002/2013GL058373.

Received 7 NOV 2013
Accepted 15 FEB 2014
Accepted article online 19 FEB 2014
Published online 2 APR 2014

Imaging spectroscopy- and lidar-derived estimates of canopy composition and structure to improve predictions of forest carbon fluxes and ecosystem dynamics

A. S. Antonarakis[1], J. W. Munger[2], and P. R. Moorcroft[1]

[1]Department of Organismic and Evolutionary Biology, Harvard University, Cambridge, Massachusetts, USA, [2]School of Engineering and Applied Sciences, Harvard University, Cambridge, Massachusetts, USA

Abstract The composition and structure of vegetation are key attributes of ecosystems, affecting their current and future carbon, water, and energy fluxes. Information on these attributes has traditionally come from ground-based inventories of the plant canopy within small sample plots. Here we show how imaging spectrometry and waveform lidar can be used to provide spatially comprehensive estimates of forest canopy composition and structure that can improve the accuracy of the carbon flux predictions of a size-structured terrestrial biosphere model, reducing its root-mean-square errors from 85%–104% to 37%–57%. The improvements are qualitatively and quantitatively similar to those obtained from simulations initialized with ground measurements and approximately double the estimated rate of ecosystem carbon uptake as compared to a potential vegetation simulation. These results suggest that terrestrial biosphere model simulations can utilize modern remote-sensing data on vegetation composition and structure to improve their predictions of the current and near-term future functioning of the terrestrial biosphere.

1. Introduction

Diagnosing the current state of terrestrial ecosystems is central to forecasting how terrestrial ecosystems will respond to changes in climate, CO_2, and other environmental forcings over the coming decades [*Friedlingstein et al.*, 2006] and to plans for monitoring and managing terrestrial carbon stocks [*Michalak et al.*, 2011; *UN-REDD*, 2011]. Terrestrial biosphere models are an integral part of these activities; however, recent analyses have shown that their predictions of terrestrial carbon stocks and fluxes generally have high degrees of uncertainty and error [*Friedlingstein et al.*, 2006; *Huntzinger et al.*, 2012]. The key to improving our understanding of current and future large-scale terrestrial ecosystem function is accurate identification and reduction of the process error in terrestrial biosphere models—errors arising from inaccuracies in their formulations embodied in their current equations and parameter values. This requires systematic comparisons of model predictions against observable metrics of ecosystem dynamics [*Braswell et al.*, 2005; *Medvigy et al.*, 2009; *Desai*, 2010; *Dietze et al.*, 2010; *Keenan et al.*, 2012; *Luo et al.*, 2012]. However, two additional important sources of error affect terrestrial biosphere model predictions. The first is forcing error: error arising from inaccuracies in the meteorological data used to drive the model simulation. The second is initialization error: error arising from the description of ecosystem's state at the beginning of the prediction period.

The impacts of forcing error are typically minimized through use of observed meteorological data as opposed to reanalysis data, or output from atmospheric models [*Medvigy et al.*, 2009]. Regarding initialization error, while not generally an issue for long-term, multi-centennial-scale simulations that are typically initialized with an arbitrary near-bare-ground ecosystem state, an accurate assessment of initial ecosystem state is important in short-term, annual-to-decadal scale simulations that are used to evaluate the predictive capabilities of terrestrial biosphere models. This includes the ability to capture observed patterns of seasonal and inter-annual variability in net ecosystem productivity [e.g., *Schwalm et al.*, 2010] and when terrestrial biosphere models are used to diagnose and assess current and near-term future ecosystem function, such as the current and future rates of carbon accumulation on landscapes [e.g., *Albani et al.*, 2010].

The most commonly used approaches to initializing short-term terrestrial biosphere model simulations have either been to use a potential vegetation condition, obtained by conducting a long-term simulation of the

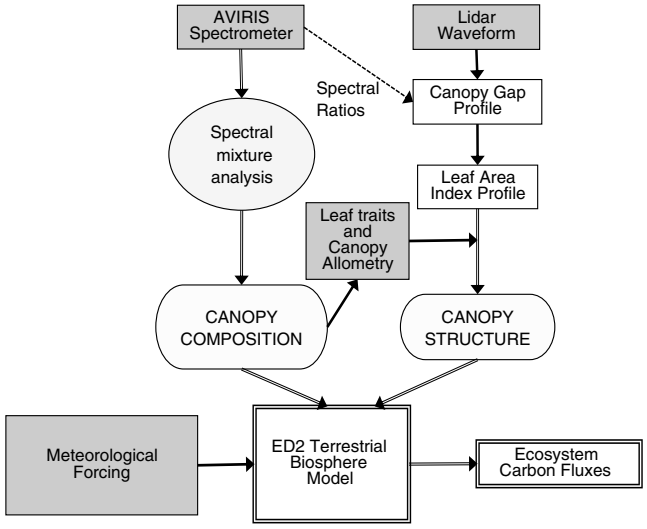

Figure 1. Flowchart outlining the derivation of forest structure and composition from Laser Vegetation Imaging Sensor waveform lidar and the Airborne Visible/Infrared Imaging Spectrometer (AVIRIS) imaging spectrometer. Spectral mixture analysis is used to derive the relative abundance composition of the different plant functional types from the imaging spectrometer measurements. The leaf area index profile is determined from the lidar-derived estimate of the canopy gap profile. Canopy structure is then calculated by relating the lidar-derived leaf area index profile to the spectrometry-derived composition and information about the leaf traits and canopy allometry of the different plant functional types. The remote-sensing estimates of canopy composition and structure are used to initialize the Ecosystem Demography (ED2) biosphere model to calculate remote-sensing-constrained estimates of the ecosystem's carbon fluxes.

model from a near-bare-ground state and forcing the model with appropriate near-surface meteorological forcing until it reaches a near steady-state condition [e.g., *Heimann et al*., 1998; *Ricciuto*, 2008; *Schwalm et al*., 2010; *Schaefer et al*., 2012], or by conducting a long-term simulation and forcing the model with historical estimates of near-surface meteorological forcing, CO_2 concentrations, and disturbance history [e.g., *Hurtt et al*., 2002; *Albani et al*., 2006; *Huntzinger et al*., 2012]. These approaches to specifying ecosystem state at the beginning of a desired prediction period are inherently problematic, however, because the ecosystem states generated are unlikely to be accurate due to the errors in model formulation (process error), errors in the long-term climate history, and a lack of knowledge of the human and natural disturbances that the ecosystem has experienced in the past (i.e., forcing error).

As shown in recent studies [*Medvigy et al*., 2009; *Hurtt et al*., 2010], ground-based inventories can be used to provide an empirical estimate of the current structure and composition of the aboveground ecosystem. Unfortunately, such ground measurements are limited in their spatial extent, and there is often a lack of consistency in measurement practices between locations [*Hurtt et al*., 2004; *Antonarakis et al*., 2011]. New remote-sensing technologies offer the promise of large-scale, spatially consistent information on the structure and composition of terrestrial plant canopies than can constrain terrestrial biosphere model predictions.

In this study, we show how comprehensive and spatially consistent remote-sensing information can be used to improve terrestrial biosphere model estimates of the existing and near-term state of the terrestrial carbon cycle by providing information on the state of the aboveground ecosystem. Building on earlier work that incorporated remote-sensing estimates of canopy height from lidar and canopy biomass from radar into terrestrial biosphere model simulations [*Hurtt et al*., 2004; *Antonarakis et al*., 2011], we show how imaging spectrometry and waveform lidar can be combined to provide sufficiently detailed, accurate, and spatially comprehensive measurement of canopy composition and structure that can be used to constrain terrestrial biosphere model predictions of the current and future terrestrial carbon fluxes. The composition of the forest canopy at Harvard Forest Long-Term Ecological Research (LTER) site was estimated from Airborne Visible/Infrared Imaging Spectrometer (AVIRIS) imaging spectrometer. The associated horizontal and vertical structure of the canopy was then estimated from Laser Vegetation Imaging Sensor (LVIS) waveform lidar measurements. A summary of the methodology is given in Figure 1. Further details can be found in the subsequent Methods section and in the supporting information.

2. Methods

The airborne lidar measurements used in this study come from LVIS [*Blair et al*., 1999], flown over Harvard Forest in July 2003, with a resulting footprint diameter of 20 m, and a 30 cm vertical and 1 m horizontal geolocation accuracy [*Hofton et al*., 2000]. The imaging spectrometry measurements come from AVIRIS that was

flown over Harvard Forest in early September 2002, acquiring measurements at a spatial resolution of 3.3 m in 224 calibrated spectral bands from 400 to 2500 nm [*Green et al*., 1998]. Harvard Forest is located in a mixed temperate forest in Central Massachusetts dominated by red oak (*Quercus rubra*), red maple (*Acer rubrum*), hemlock (*Tsuga canadensis*), red pine (*Pinus resinosa*), and white pine (*Pinus strobus*). The Harvard flux-tower sites—consisting of the Environmental Measurement Site (EMS) [*Munger and Wofsy*, 1999], Hemlock (HEM) flux tower [*Foster and Barker-Plotkin*, 1999], and the Little Prospect Hill (LPH) flux tower [*Hadley*, 2009]—exhibit significant differences in their structure and composition. In addition to measurements of carbon fluxes, the three flux-tower sites also have extensive forest inventory plots within their flux-tower footprints (see supporting information).

The terrestrial biosphere model used in this study was the Ecosystem Demography (ED2) model [*Moorcroft et al*., 2001; *Medvigy et al*., 2009] that is able to incorporate information on fine-scale variation in the vertical and horizontal structure and composition of plant canopies. Canopy composition within the ED2 model is represented as a series of plant functional types (PFTs) that have different biophysical, physiological, morphological, and ecological properties. Following earlier work [*Albani et al*., 2006; *Medvigy et al*., 2009], the ecosystem composition at Harvard Forest was represented as a mixture of five PFTs: early-, mid-, and late-successional deciduous trees, and early- and late-successional conifers [*Medvigy et al*., 2009]. The relative abundance of these different PFTs for the three Harvard Forest sites was determined from AVIRIS using Multiple Endmember Spectral Mixture Analysis [*Roberts et al*., 1998], which allows the number of pure pixels (end-members) initially defined as belonging to a PFT to vary during the un-mixing process on a pixel-by-pixel basis (see supporting information). The resulting abundance of the different PFTs is estimated in terms of percentages within each pixel. An alternate method, in which the PFTs were distinguished using regressions relating spectra to leaf traits [*Martin and Aber*, 1997; *Martin et al*., 1998], yielded similar results (see supporting information).

The leaf area index profiles of individual pulses (LAI(h)) was estimated from the lidar gap fraction [*Ni-Meister et al*., 2001] (see supporting information, Eq.s S1–S3). Forest structure and composition were then estimated by combining the lidar-derived LAI profiles with the AVIRIS-derived estimates of PFT composition by relating them to the size distribution of trees of the different PFTs across horizontal space. Consistent with its representation in the ED2 model, the size distribution of the different PFTs (i) within each pixel location x is given by $n^i(h,x)$, the density profile (number per area) of trees of type i as a function tree height h. $n^i(h,x)$ can be related to the leaf area index profile (LAI(h,x)), by calculating the foliage area per plant (i.e., PFT-dependent specific leaf area (SLA^i) and leaf biomass ($B^i_{leaf}(h)$) as specified in the ED2 model (see supporting information, Eq.s S4–S8)). In order to initialize the ED2 model, the tree density with height ($n^i(h,x)$) of each PFT i was translated into a corresponding diameter size distribution ($n^i(z,x)$) using the height-to-diameter allometry used in the ED2 model. The resulting site-level size class distributions and basal areas for the EMS, HEM, and LPH sites were calculated by averaging the diameter size-class distributions of the pixels whose locations matched those of the ground-based survey plots at each site.

3. Results

The remote-sensing-based estimates of the composition and structure are summarized in Figure 2, which shows the PFT composition (panel a) and basal area (panel b) of the forest canopy across the Prospect Hill region of Harvard Forest LTER. The combination of imaging spectrometry and lidar remote sensing captures the observed spatial variation in structure and composition for the 82 forest inventory plots around the EMS, LPH, and HEM flux-tower sites (Figure 2d; R^2 of 0.672, and a root-mean-square error (RMSE) of approximately 10 m^2/ha).

The remote-sensing-derived diameter size-class distributions for the three flux-tower sites are shown in Figure 3. As can be seen in the figure, the remote-sensing measurements capture the observed differences in forest composition and structure at the flux-tower sites. Estimates of the basal areas for the EMS, LPH, and HEM flux-tower footprints were within 2.5–5.8 m^2/ha (8–33%) of the ground-based estimates of 33.5, 17.3, and 49.7 m^2/ha, respectively. The remote-sensing measurements also captured the associated differences in canopy composition, including the dominance of mid-successional hardwoods at the EMS and LPH sites, and the relative abundances of early- and late-successional conifers at the HEM site. The distribution of early-successional conifers in the remote-sensing measurements is, however, less skewed toward the larger size

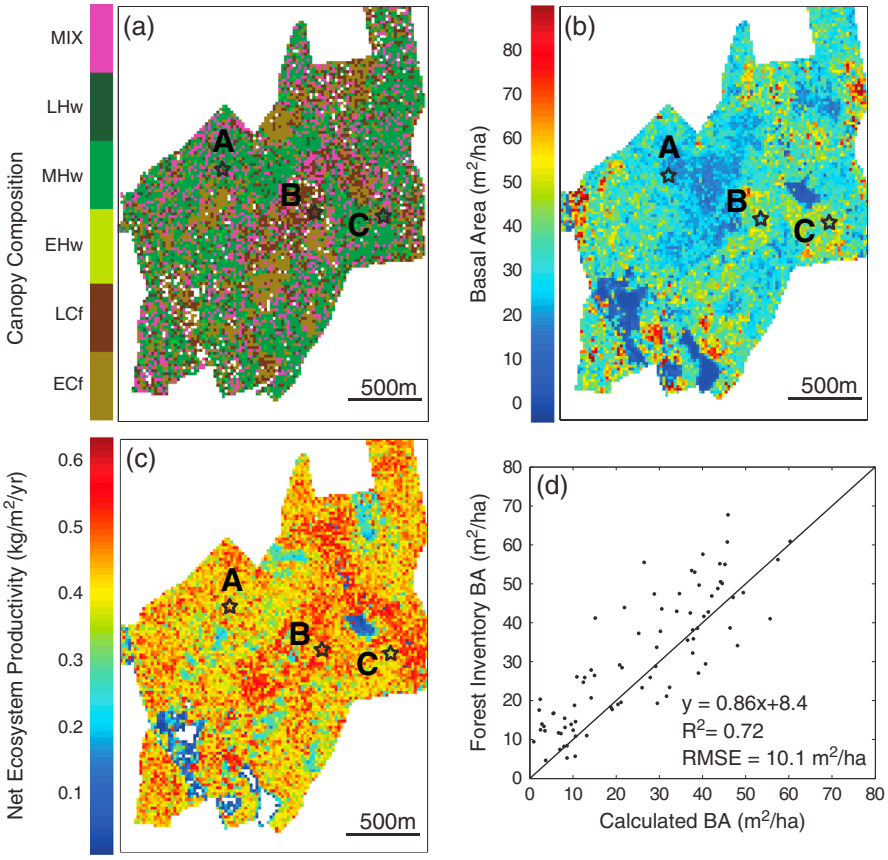

Figure 2. Spatial variation in forest composition, structure, and carbon fluxes across the Prospect Hill Tract at Harvard Forest, MA. (a) Spatial variation in the abundance of the five plant functional types (PFTs) as estimated from the AVIRIS imaging spectrometer: colors indicate forest stands that are dominated by early-successional conifers (ECf), late-successional conifers (LCf), early-successional hardwoods (EHw), mid-successional hardwoods (MHw), and late-successional hardwoods (LHw), (meaning that the PFT constitutes more than 40% of the basal area at that location), as well as locations in which several PFTs are co-dominant (MIX). (b) Remote-sensing-derived total basal area (m^2/ha). (c) Net ecosystem productivity (kg/m^2/yr) as estimated from the remote-sensing constrained terrestrial biosphere model. The letters A, B, and C show positions of the LPH, HEM, and EMS flux towers, respectively. Pixels are 20 × 20 m. The remote-sensing-constrained estimate of the average NEP of stands within the region is 3.96 TC/ha/yr, and the total Prospect Hill Tract has a carbon storage of ~1400 TC/yr. The total carbon storage from the potential vegetation-initialized simulation is ~700 TC yr^{-1}. Figure 2d shows the remote-sensing-derived estimates of forest basal area (BA) compared to ground-based forest inventory measurements at the 40 plots at the EMS site, the 12 plots at the HEM site, and the 30 plots at the LPH site. The 1:1 line (black line) is also shown.

classes compared to the ground-based observations (Figures 3e and 3f). An assessment of the plot-level accuracy of the composition estimates can be found in Figure S2.

The remote-sensing-derived estimates of forest structure and composition were used to initialize a series of terrestrial biosphere model simulations for the three flux-tower sites. The predictions of these simulations were then compared against the observed fluxes and against model simulations initialized with either the ground-based forest inventory measurements, or output from a potential vegetation simulation. Further details on the model initialization and simulation procedures can be found in the supporting information.

Figures 4 and 5 show the predicted and observed patterns of net ecosystem productivity (NEP) and gross primary productivity (GPP) at the three flux-tower sites. As the figures show, both the seasonal and inter-annual predictions from the potential vegetation initialized simulations (grey lines) are considerably different than the observed patterns of NEP and GPP observed at all three flux towers. The 6-year average NEP derived from the potential vegetation simulation was 0.19 kgC$m^{-2}yr^{-1}$, compared to the observed fluxes at the EMS, LPH, and HEM flux towers that were 0.47, 0.43, and 0.63 kgC$m^{-2}yr^{-1}$, respectively (RMSEs of the annual NEP values are 0.44, 0.45, and 0.54 kgC$m^{-2}yr^{-1}$, respectively). Similarly, the average GPP in the potential

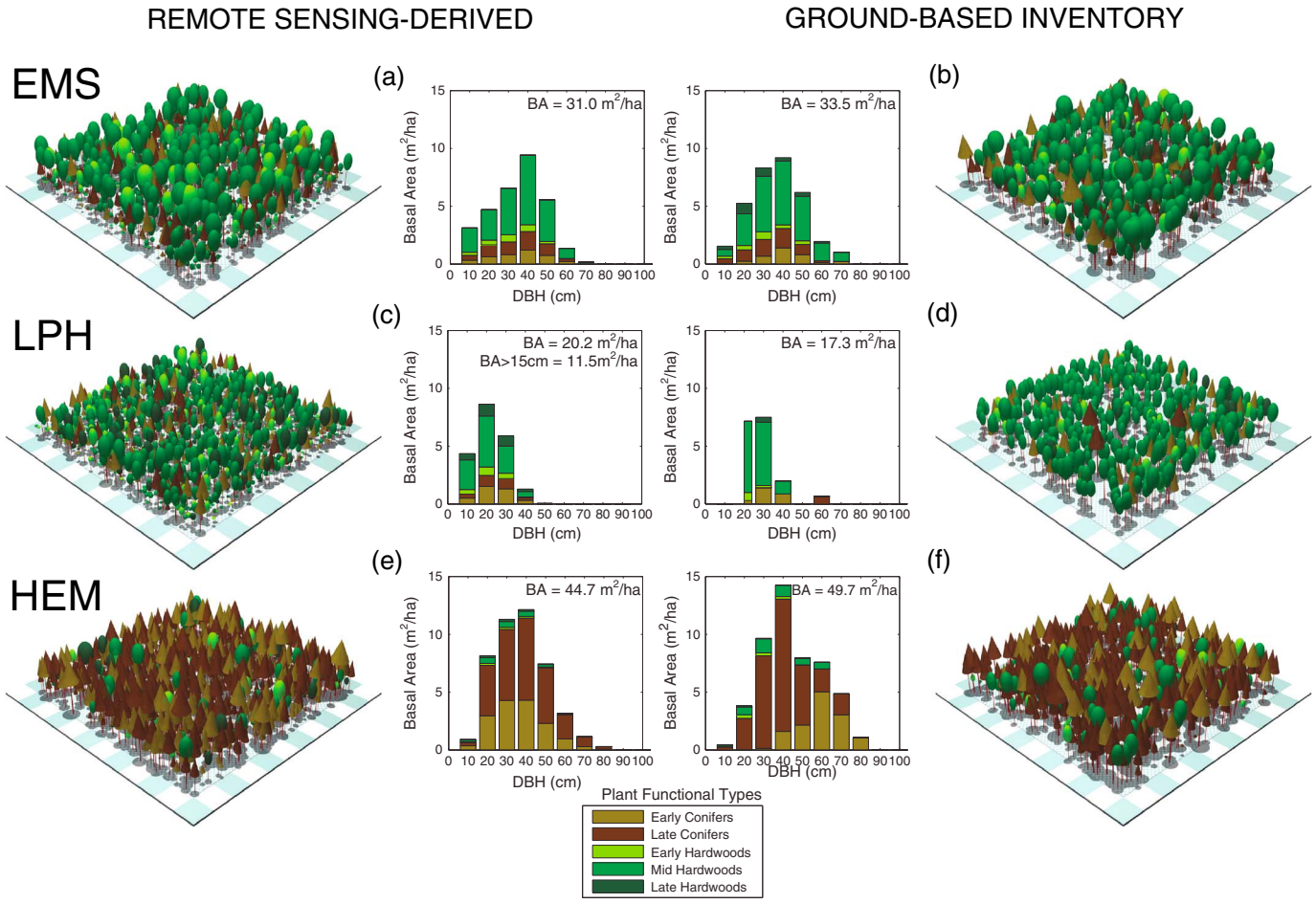

Figure 3. (Left-hand panels) Remote-sensing-derived and (right-hand panels) ground-based inventory measurements of forest ecosystem structure and composition for the (a,b) EMS, (c,d) LPH, and (e,f) HEM sites. Forest visualizations and total basal area (BA) of each site are also shown. The size distribution in Figure 3d is truncated because trees less than 15 cm diameter were not measured at the LPH site.

vegetation simulation was 2.9 $kgCm^{-2}yr^{-1}$, while the 6-year averages from the EMS, LPH, and HEM flux towers were 1.6, 1.2, and 1.5 $kgCm^{-2}yr^{-1}$, respectively (RMSEs of 1.4, 1.75, and 1.45 $kgCm^{-2}yr^{-1}$, respectively).

Simulations initialized from either the ground-based inventory measurements or the remote-sensing measurements had substantially improved predictions of seasonal and inter-annual carbon fluxes (Figures 4 and 5). NEP estimates obtained with the ground-based initialized simulations were 0.49, 0.32, and 0.56 $kgCm^{-2}yr^{-1}$ for the EMS, LPH, and HEM sites (RMSEs of 0.28, 0.26, and 0.24 $kgCm^{-2}yr^{-1}$), while those obtained from the remote-sensing-based initialized simulations were 0.49, 0.27, and 0.59 $kgCm^{-2}yr^{-1}$ (RMSEs of 0.27, 0.24, and 0.23 $kgCm^{-2}yr^{-1}$). Similarly, the average GPP values predicted by the ground-based initialized simulations were 1.6, 1.3, and 2.0 $kgCm^{-2}yr^{-1}$ for the EMS, LPH, and HEM sites (RMSEs 0.28, 0.29, and 0.49 $kgCm^{-2}yr^{-1}$), while those predicted by the remote-sensing-based initialized simulations were 1.6, 1.0, and 2.2 $kgCm^{-2}yr^{-1}$ (RMSEs 0.28, 0.30, and 0.65 $kgCm^{-2}yr^{-1}$). These improved estimates of NEP ecosystem productivity significantly impact the estimated rate of carbon storage by the ecosystem. The carbon storage of the total Prospect Hill Tract estimated from the potential vegetation-initialized simulation is ~700 $TC\,yr^{-1}$, while the remote-sensing constrained estimate is ~1400 $TC\,yr^{-1}$.

4. Conclusions

The key finding of this study is that a strategic combination of waveform lidar and imaging spectrometry can provide sufficiently accurate measurements of fine-scale forest structure and composition to improve the accuracy of short-term terrestrial biosphere model simulations of ecosystem function. As seen in Figures 4

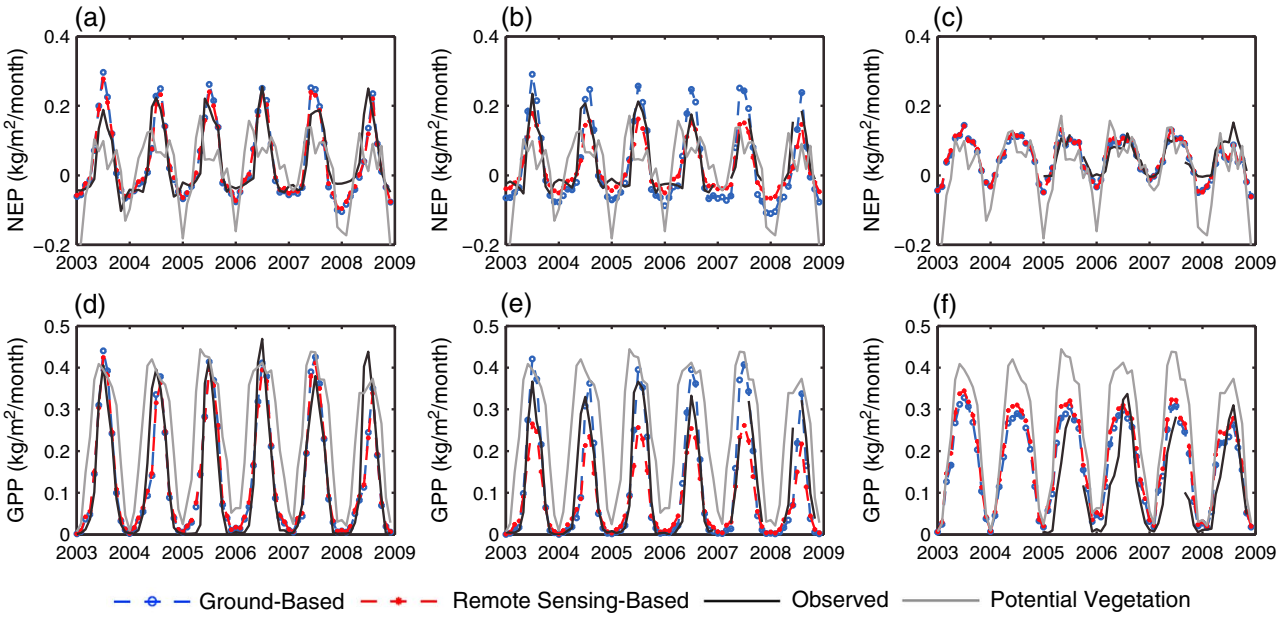

Figure 4. Seasonal net ecosystem productivity (NEP) and gross primary productivity (GPP) predictions obtained from ground inventory-initialized, remote-sensing-initialized, and potential vegetation-initialized simulations of the ED2 terrestrial biosphere model compared to the fluxes observed at the (a,d) EMS, (b,e) LPH, and (c,f) HEM flux-tower sites.

and 5, the improvements in accuracy seen in the remote-sensing-initialized simulations closely resemble those obtained in simulations initialized with ground-based measurements. These, combined with the results shown in Figures 2d and 3, indicate that the improved accuracy of the remote-sensing initialized simulation is not fortuitous but rather is arising from the more accurate description of aboveground ecosystem state. This ability to use lidar and imaging spectrometry to initialize short-term terrestrial biosphere model simulations is important because these instruments can provide a spatially comprehensive estimate of the actual aboveground ecosystem state, rather than either requiring detailed ground observations, or assuming, as is current practice, that vegetation is in equilibrium with its current climate, or that its climate forcing and disturbance history is accurately known. The improvement in the accuracy of the net carbon fluxes predicted by the remote-sensing-initialized model can be seen by comparing its estimates against the carbon fluxes estimated from a model initialized with output from a potential vegetation simulation. As seen in Figures 5a–5c, the incorporation of the remote-sensing measurements considerably improves the model's

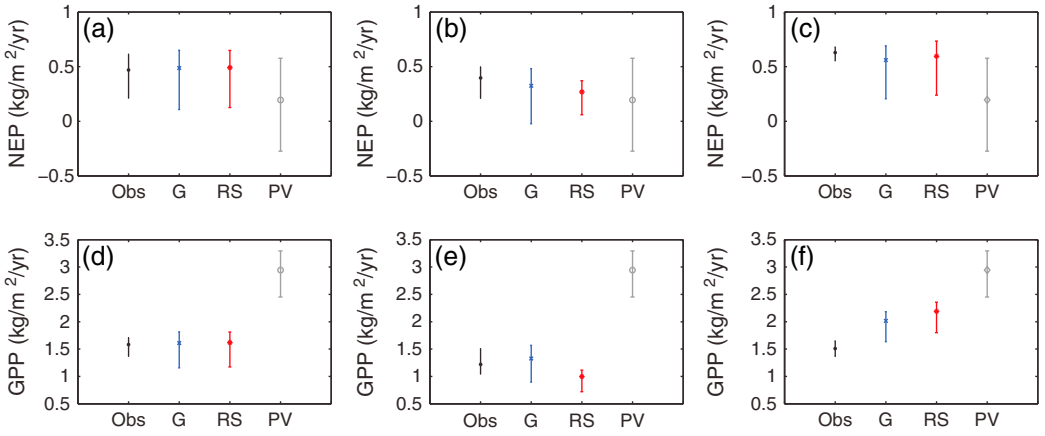

Figure 5. Average and inter-annual variability in net carbon ecosystem productivity (NEP) and gross primary productivity (GPP) predictions obtained from ground inventory-initialized (G), remote-sensing-initialized (RS), and potential vegetation-initialized (PV) simulations of the ED2 terrestrial biosphere model for the period 2003–2009 compared to the observed fluxes (Obs) at the (a,d) EMS, (b,e) LPH, and (c,f) HEM flux-tower sites.

predictions of carbon fluxes at the three sites (see Figures 5a–5c), reducing the RMSEs of the annual carbon flux estimates from 85%–104% to 37%–57%.

This study offers a relatively simple and straightforward method to estimate current aboveground ecosystem state from modern remote-sensing measurements. As shown in Figure 3, the remote-sensing derived forest structure and composition capture the observed variation in the size class distributions at the three evaluation sites. There are, however, two discrepancies. First, close inspection of Figure 2d shows that there is a small but noticeable tendency for the remote-sensing estimate of canopy structure to underestimate the total basal area. This was particularly true at LPH, where the remote-sensing derived total basal area for trees $>$15 cm at LPH was 5.8 m^2/ha lower than the ground-based estimate (Figure 3d), and as a result, the remote-sensing-initialized estimate of GPP at LPH was significantly lower than the observed fluxes (Figure 4e). Second, the skewed distribution of the early-successional conifers toward larger size classes at the HEM site (Figure 3f) is not reflected in the remote-sensing estimate (Figure 3e). Several factors may contribute to these discrepancies: (i) a possible bias in the diameter-height allometry, which, when applied to the estimated tree density versus height relationship, shifts the size distribution toward smaller sizes of individuals; (ii) the simplifying assumptions used in the composition estimation algorithm, namely, that individuals within a given height class have similar crown sizes (and thus tree density is proportional to the imaging spectrometry-derived estimate of foliage cover), and that the composition estimate for each 20 m pixel is applied across all height classes within the profile.

The results from this study suggest that regional-scale terrestrial ecosystem and biosphere model simulations can be constrained with active and passive remote-sensing data to produce more accurate predictions of how terrestrial ecosystems will change in the future. In the case of the aggrading forest ecosystems found at Harvard Forest that have been analyzed here, the levels of accuracy achieved in this study (in which forest basal area was estimated to within 2.5–5.8 m^2/ha of the ground-based estimates) reduced the RMSEs of annual carbon flux estimates from 85%–104% to 37%–57%. The magnitude of the improvements that will occur in other ecosystems is, at present, unclear since the quantitative relationship between improved estimates of forest structure and composition and resulting estimates of ecosystem carbon fluxes is likely to be complex, varying depending on ecosystem type, its successional state, and its current meteorological forcing. Constraining models at larger scales will require broader coverage of imaging spectrometry and lidar data [e.g., *Asner et al*., 2007, 2010; *Levick and Asner*, 2013]. Recent results suggest that interferometric radar, which has the capability of determining canopy height profiles similar to lidar waveform measurements, may also be used to measure the structure of forest canopies [*Walker et al*., 2007; *Treuhaft et al*., 2009]. An important avenue for improving remote-sensing-derived estimates of forest composition may come from detailed considerations of leaf spectral properties. Although the mechanistic basis of some of the relationships are debated [*Knyazikhin et al*., 2013], recent work in tropical forests [*Asner and Martin*, 2009, 2011] has shown that spectral signatures of tree species can be related to a variety of leaf traits, including specific leaf area, light saturated rate of photosynthesis, and leaf nitrogen content—traits that are commonly used to define PFTs of terrestrial biosphere models. The ability shown here to provide airborne and satellite remotely sensed empirical constraint on current aboveground state of terrestrial ecosystems promises to improve the ability to correctly diagnose, and correct, process-error in terrestrial biosphere models, improved estimation of the regional carbon budgets, and improved seasonal to multi decadal-scale forecasts of terrestrial ecosystem change.

Acknowledgments

The authors would like to acknowledge the NASA Earth Science Research Program NNH05ZDA001N-RSSCC grant "Remote Sensing Science for Carbon and Climate," and NNH11ZDA001N-HYSPIRI grant "Linking Terrestrial Biosphere Models with Remote Sensing Measurements of Ecosystem Composition, Structure, and Function." We thank Bryan Blair and Michelle Hofton for the processing of the LVIS data. Our special thanks go to Steve Wofsy, Audrey Barker-Plotkin, Julien Hadley, David Foster, Mary Martin, John Aber, and the Harvard Forest LTER for their generosity in providing us with the eddy-flux tower and ground-based forest inventory measurements that were used to evaluate the remote-sensing-based estimation methods developed in this paper.

The Editor thanks two anonymous reviewers for their assistance in evaluating this paper.

References

Albani, M., D. Medvigy, G. C. Hurtt, and P. R. Moorcroft (2006), The contributions of land-use change, CO_2 fertilization, and climate variability to the Eastern US carbon sink, *Global Change Biology*, *12*, 2370–2390.

Albani, M., P. R. Moorcroft, A. M. Ellison, D. A. Orwig, and D. R. Foster (2010), Predicting the impact of hemlock woolly adelgid on carbon dynamics of eastern United States forests, *Can. J. For. Res.*, *40*(1), 119–133.

Antonarakis, A. S., S. S. Saatchi, R. L. Chazdon, and P. R. Moorcroft (2011), Using Lidar and Radar measurements to constrain predictions of forest ecosystem structure and function, *Ecol. Appl.*, *21*, 1120–1137.

Asner, G. P., and R. E. Martin (2009), Airborne spectranomics: Mapping canopy chemical and taxonomic diversity in tropical forests, *Frontiers Ecol. Environ.*, *7*, 269–276.

Asner, G. P., and R. E. Martin (2011), Canopy phylogenetic, chemical and spectral assembly in a lowland Amazon forest, *New Phytol.*, *189*, 999–1012.

Asner, G. P., D. E. Knapp, T. Kennedy-Bowdoin, M. O. Jones, R. E. Martin, J. Boardman, and C. B. Field (2007), Carnegie airborne observatory: In-flight fusion of hyperspectral imaging and waveform light detection and ranging for three-dimensional studies of ecosystems, *J. Appl. Remote Sens.*, *1*, 013,536.

Asner, G. P., et al. (2010), High-resolution forest carbon stocks and emissions in the Amazon, *Proc. Natl. Acad. Sci. U.S.A.*, *107*, 16,738–16,742.

Blair, J. B., D. L. Rabine, and M. A. Hofton (1999), The laser vegetation imaging sensor (LVIS): A medium-altitude, digitations-only, laser altimeter for mapping vegetation and topography, *ISPRS J. Photogramm. Remote Sens.*, *54*, 115–122.

Braswell, B. H., W. J. Sacks, E. Linder, and D. S. Schimel (2005), Estimating diurnal to annual ecosystem parameters by synthesis of a carbon flux model with eddy covariance net ecosystem exchange observations, *Global Change Biol.*, *11*, 335–355.

Desai, A. K. (2010), Climatic and phenological controls on coherent regional interannual variability of carbon dioxide flux in a heterogeneous landscape, *J. Geophys. Res.*, *115*, G00J02, doi:10.1029/2010JG001423.

Dietze, M. C., et al. (2010), Characterizing the performance of ecosystem models across time scales: A spectral analysis of the North American Carbon Program site-level synthesis, *J. Geophys. Res.*, *116*, G04029, doi:10.1029/2011JG001661.

Foster, D., and A. Barker-Plotkin (1999), Hemlock mapped tree plot. Harvard Forest Data Archive: HF031. [Available at http://harvardforest.fas.harvard.edu:8080/exist/xquery/data.xq?id=hf031.]

Friedlingstein, P., et al. (2006), Climate–carbon cycle feedback analysis: Results from the C4MIP model intercomparison, *J. Clim.*, *19*, 3337–3353.

Green, R. O., et al. (1998), Imaging spectroscopy and the Airborne Visible/Infrared Imaging Spectrometer (AVIRIS), *Remote Sens. Environ.*, *65*, 227–248.

Hadley, J. (2009), HEM and LPH towers - Tree growth and above-ground biomass. Harvard Forest Data Archive: HF149. [Available at http://harvardforest.fas.harvard.edu:8080/exist/xquery/data.xq?id=hf149.]

Heimann, M., et al. (1998), Evaluation of terrestrial carbon cycle models through simulations of the seasonal cycle of atmospheric CO_2: First results of a model inter- comparison study, *Global Biogeochem. Cycles*, *12*, 1–24, doi:10.1029/97GB01936.

Hofton, M. A., J. B. Blair, J. B. Minister, J. R. Ridgeway, N. P. Williams, J. L. Bufton, and D. L. Rabine (2000), An airborne scanning laser altimeter survey in Long Valley, California, *Int. J. Remote Sens.*, *21*, 2413–2437.

Huntzinger, D. N., et al. (2012), North American Carbon Program (NACP) regional interim synthesis: Terrestrial biospheric model intercomparison, *Ecol. Modell.*, *232*, 144–157.

Hurtt, G. C., S. W. Pacala, P. R. Moorcroft, J. P. Caspersen, E. Shevliakova, and B. Moore (2002), Projecting the future of the US carbon sink, *Proc. Natl. Acad. Sci. U.S.A.*, *99*, 1389–1394.

Hurtt, G. C., R. Dubayah, J. Drake, P. R. Moorcroft, S. W. Pacala, J. B. Blair, and M. G. Fearon (2004), Beyond potential vegetation: Combining Lidar data and a height-structured model for carbon studies, *Ecol. Appl.*, *14*(3), 873–883.

Hurtt, H. C., J. Fisk, R. Q. Thomas, R. Dubayah, P. R. Moorcroft, and H. H. Shugart (2010), Linking models and data on vegetation structure, *J. Geophys. Res.*, *115*, G00E10, doi:10.1029/2009JG000937.

Keenan, T. F., et al. (2012), Terrestrial biosphere model performance for inter-annual variability of land-atmosphere CO_2 exchange, *Global Change Biol.*, *18*, 1971–1987.

Knyazikhin, Y., et al. (2013), Hyperspectral remote sensing of foliar nitrogen content, *Proc. Natl. Acad. Sci. U.S.A.*, *110*, E185–192.

Levick, S. R., and G. P. Asner (2013), The rate and spatial pattern of treefall in a savanna landscape, *Biol. Conservation*, *157*, 121–127.

Luo, Y. Q., et al. (2012), A framework for benchmarking land models, *Biogeosciences*, *9*, 3857–3874.

Martin, M. E., and J. D. Aber (1997), High spectral resolution remote sensing of forest canopy lignin, nitrogen, and ecosystem processes, *Ecol. Appl.*, *7*(2), 431–443.

Martin, M. E., S. D. Newmand, J. D. Aber, and R. G. Congalton (1998), Determining forest species composition using high spectral resolution remote sensing data, *Remote Sens. Environ.*, *65*, 249–254.

Medvigy, D., S. C. Wofsy, J. W. Munger, D. Y. Hollinger, and P. R. Moorcroft (2009), Mechanistic scaling of ecosystem function and dynamics in space and time: Ecosystem Demography model version 2, *J. Geophys. Res.*, *114*, G01002, doi:10.1029/2008JG000812.

Michalak, A. M., R. B. Jackson, G. Marland, C. L. Sabine, and the Carbon Cycle Science Working Group (2011), A U.S. carbon cycle science plan. United States Carbon Cycle Carbon Planning. [Available at http://www.carboncyclescience.gov/sites/default/files/documents/USCarbonCycleSciencePlan-2011.pdf.]

Moorcroft, P. R., G. C. Hurtt, and S. W. Pacala (2001), A method for scaling vegetation dynamics: The Ecosystem Demography Model (ED), *Ecol. Monogr.*, *71*(4), 557–585.

Munger, W., and S. Wofsy (1999), EMS - Biomass inventories. Harvard Forest Data Archive: HF069. [Available at http://harvardforest.fas.harvard.edu:8080/exist/xquery/data.xq?id=hf069.]

Ni-Meister, W., D. L. B. Jupp, and R. Dubayah (2001), Modeling lidar waveforms in heterogeneous and discrete canopies, *IEEE Trans. Geosci. Remote Sens.*, *39*, 1943–1958.

Ricciuto, D. (2008), Protocol for the North American Carbon Project (NACP) site-level interim synthesis model-data comparison (site synthesis), Version 7. Oak Ridge National Laboratory, Oak Ridge, Tenn. [Available at http://nacp.ornl.gov/mast-dc/docs/Site_Synthesis_Protocol_v7.pdf.]

Roberts, D. A., M. Gardner, R. Church, S. Ustin, G. Scheer, and R. O. Green (1998), Mapping Chaparral in the Santa Monica Mountains using multiple endmember spectral mixture models, *Remote Sens. Environ.*, *65*, 267–279.

Schaefer, K., et al. (2012), A model-data comparison of gross primary productivity: Results from the North American carbon program site synthesis, *J. Geophys. Res.*, *117*, G03010, doi:10.1029/2012JG001960.

Schwalm, C. R., et al. (2010), A model-data intercomparison of CO_2 exchange across North America: Results from the North American Carbon Program site synthesis, *J. Geophys. Res.*, *115*, G00H05, doi:10.1029/2009JG001229.

Treuhaft, R. N., B. D. Chapman, J. R. dos Santos, F. G. Goncalves, L. V. Dutra, P. M. L. A. Graca, and J. B. Drake (2009), Vegetation profiles in tropical forests from multibaseline interferometric synthetic aperture radar, field, and lidar measurements, *J. Geophys. Res.*, *114*, D23110, doi:10.1029/2008JD011674.

UN-REDD (2011), UN-REDD programme strategy 2011-2015. [Available at http://www.un-redd.org/PublicationsResources/tabid/587/Default.aspx.]

Walker, W. S., J. M. Kellndorfer, and L. E. Pierce (2007), Quality assessment of SRTM C- and X-band interferometric data: Implications for the retrieval of vegetation canopy height, *Remote Sens. Environ.*, *106*, 428–448.